Nonlinear Analysis: Modelling and Control, Vol. 27, No. 4, 669–683
https://doi.org/10.15388/namc.2022.27.26678

Dufour and Soret effects on pulsatile hydromagnetic flow of Casson fluid in a vertical non-Darcian porous space

Suripeddi Srinivas[a], **Challa Kalyan Kumar**[b,1], **Anala Subramanyam Reddy**[c]

[a]Department of Mathematics, School of Advanced Sciences, VIT-AP University, Inavolu, Vijayawada-522237, India

[b]Department of Mathematics, Narayana Engineering College, Gudur, SPSR Nellore-524101, India
kalyankumar.challa@gmail.com

[c]Department of Mathematics, School of Advanced Sciences, Vellore Institute of Technology, Vellore-632014, India

Received: July 26, 2021 / **Revised:** January 31, 2022 / **Published online:** April 11, 2022

Abstract. This article aims to inspect the pulsating hydromagnetic slip flow of Casson fluid in a vertical porous channel with heat and mass transfer. The fluid is injected into the channel from the left wall and removed at the opposite wall with the same velocity. The impact of non-Darcy, Soret, and Dufour effects are taken under consideration. The governing partial differential equations (PDEs) are converted to ordinary differential equations (ODEs) using perturbation method and solved by utilizing 4th-order Runge–Kutta (R–K) technique together with shooting method. The impact of dissimilar parameters on flow, heat and mass transfer characteristics are displayed and discussed.

Keywords: Casson fluid, slip parameter, pulsatile flow, convective boundary, Dufour and Soret effects.

1 Introduction

Studies pertaining to the MHD flows of non-Newtonian fluids in a porous medium are important because of its applications in irrigation problems, process of petroleum, heat-storage beds, paper, textile, and polymer composite industries. The most famous among these fluids is Casson fluid. Casson fluid model was introduced by Casson [4] for prediction of the flow behaviour of pigment-oil suspensions in lithographic varnishes. We can characterize Casson fluid as a shear thinning liquid which is considered to have an infinite viscosity at zero rate of shear, a yield stress below which no flow occurs, and a zero viscosity at an infinite rate of shear. The examples of Casson fluid are concentrated fruit juices, honey, tomato sauce, jelly, and human blood [8, 10, 14, 17]. Chamkha [7] investigated

[1]Corresponding author.

the hydromagnetic fully developed laminar mixed convection flow in a vertical channel with symmetric and asymmetric wall heating conditions in the presence or absence of heat generation or absorption effects. Loganathan and Deepa [21] researched the EMHD flow of the Casson fluid on a permeable Riga-plate. Pantokratoras [25] investigated the natural convection of non-Newtonian power-law fluids over a vertical plate. Walawender et al. [33] employed Casson model for portraying blood flow curves.

Pulsatile flow in a porous pipe or a channel is an important study due to its application in both engineering systems (microelectromechanical systems or MEMS, pulse combustors, IC engines, and reciprocating pumps) and natural systems (vascular diseases, respiratory systems, circulatory systems). Especially, the pulsatile flow in a porous channel is significant in the dialysis of blood in artificial kidneys [1, 3, 16, 19, 26]. Chamkha [6] examined the problem of flow and heat transfer of two electrically conducting and heat generating or absorbing immiscible fluids in a vertical infinitely long channel in the presence or absence of a porous medium and applied magnetic field. Kumar et al. [20] analyzed the problem of fully-developed convective flow of a micropolar and viscous fluid between parallel plate vertical channels with asymmetric wall temperature distribution. Celli and Kuznetsov [5] investigated the pulsatile viscous flow inside a horizontal infinitely wide channel. Haddad et al. [12] examined the pulsating laminar and incompressible fully developed pipe flows. Srinivas et al. [30] studied the pulsatile flow of hydromagnetic Casson fluid in a porous channel. Wang [34] illustrated the pulsating flow in a porous channel.

The fluids displaying boundary slip are significant in technological applications like inertial cavities and polishing of artificial heart valves [22,27,35]. The study of convective boundary condition is of extraordinary significance due to its application in engineering and industrial processes like material drying and transpiration cooling process [9, 31]. Malathy et al. [23] have elucidated the influences of slip and thermal radiation on MHD pulsatile flow of an Oldroyd-B fluid in a porous space with convective boundary condition. Sayed et al. [28] studied the peristaltic transport of nanofluid in an inclined asymmetric channel in the presence of slip and convective boundary conditions.

The energy flux caused by a concentration gradient was found in 1873 by Dufour and was correspondingly named the Dufour effect. It is additionally known as the diffusion-thermo effect. Then again, mass flux is able to be made by a temperature gradient as was recognized by Soret. This is the thermal-diffusion effect. Dufour and Soret effects assume a significant role when large density contrasts exist in the flow regime. Radiation, Dufour, and Soret effects on MHD flows emerge in applied physics and numerous areas of engineering like catalytic reactors, heat insulation, geothermal systems, MHD generators, and drying technology [13, 24, 29]. Dzulkifli et al. [11] numerically discussed the Dufour and Soret parameters on the boundary layer flow in nanofluid through shrinking/stretching sheet. Khan et al. [15] discussed the cross diffusion effects on Carreau–Yasuda fluid flow over a porous stretchable surface. Umavathi and Chamkha [32] examined the stability analysis of cross diffusion when a nanofluid saturated with porous space was filled in a horizontal channel. Recently, Kumar and Srinivas [18] performed the simulation for pulsation flow of hydromagnetic Casson fluid in a vertical channel with Dufour and Soret effects.

The literature reveals that no study related to hydromagnetic pulsatile Casson fluid in a vertical permeable channel has been explored so far. Inspired by the past investigations [1, 23, 26, 34] and keeping in the perspective on wide applications, we made an endeavour to portray the cross diffusion impacts on pulsating hydromagnetic slip flow of Casson fluid in a vertical porous channel with convective boundary. The coupled PDEs are converted to ODEs using perturbation method and solved by utilizing 4th-order R–K technique together with shooting method.

2 Formulation of the model

Consider the laminar and incompressible pulsating flow of Casson fluid between two vertical parallel walls at a distance h. The strength B_0 of a uniform magnetic field is applied opposite to the flow direction. We assume that the plates are very wide and very long, so that the flow is essentially axial. So that only $\hat{x}$-component of $\hat{u}$ of the velocity does not vanish. The condition of fully developed flow implies that $\partial\hat{u}/\partial\hat{x} = 0$. Since the velocity is solenoidal, we obtain $\partial\hat{v}/\partial\hat{y} = 0$. As a consequence, the velocity component $\hat{v}$ is constant in any channel section and is equal to zero at the channel walls, so $\hat{v}$ must be vanishing at any position. The $\hat{y}$-momentum balance equation can be expressed as $\partial\hat{p}/\partial\hat{y} = 0$ (see [2, 12, 19]). The slip parameter, Joule heating, convective boundary, Dufour and Soret effects are considered. A Cartesian coordinate system is taken so that the $\hat{x}$-axis is taken along the flow direction (vertical), and $\hat{y}$-axis is orthogonal to the walls (see Fig. 1). The channel walls possess the characteristics of convective-type boundary condition. The left and right walls maintain temperatures are T_0, T_1 ($> T_0$), and concentrations are C_0, C_1 ($> C_0$), respectively. The convective boundary conditions at the left wall and the right wall are $-\kappa\partial\hat{T}/\partial\hat{y} = h_f(\hat{T} - T_0)$ and $-\kappa\partial\hat{T}/\partial\hat{y} = h_f(\hat{T} - T_1)$, respectively. The fluid is injected into the channel from the left wall with a velocity v_0 and removed at the opposite wall with the same velocity. The stress and strain relationship is designed as (Kumar et al. [19], Loganathan and Deepa [21]):

$$\tau_{ab} = \begin{cases} (\mu_B + P_{\hat{y}}/\sqrt{2\pi_c})2e_{ab}, & \pi_c > \pi, \\ (\mu_B + P_{\hat{y}}/\sqrt{2\pi})2e_{ab}, & \pi_c < \pi. \end{cases}$$

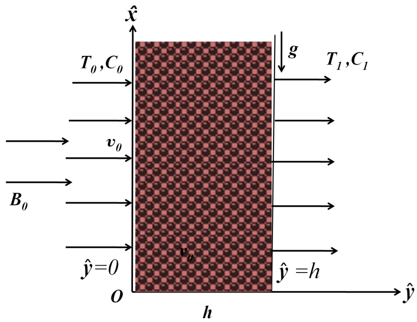

Figure 1. Schematic diagram of vertical porous channel.

The $(a,b)^{\text{th}}$ component of the deformation rate and shear stress tensor are e_{ab} and τ_{ab}, respectively. $P_{\hat{y}}$ is yield stress, π ($= e_{ab}^2$) is the product of shear rate components, π_c is the critical value of π, μ_B is the plastic dynamic viscisity. The governing equations are (Adesanya et al. [1], Radhakrishnamacharya and Maiti [26])

$$\begin{aligned}\frac{\partial \hat{u}}{\partial \hat{t}} + v_0 \frac{\partial \hat{u}}{\partial \hat{y}} &= -\frac{1}{\rho}\frac{\partial \hat{p}}{\partial \hat{x}} + \nu\left(1+\frac{1}{\beta}\right)\frac{\partial^2 \hat{u}}{\partial \hat{y}^2} + g\beta_{\hat{T}}(\hat{T}-T_0) + g\beta_{\hat{C}}(\hat{C}-C_0)\\ &\quad - \frac{\sigma B_0^2}{\rho}\hat{u} - \frac{\mu \varPhi}{\rho k}\hat{u} - \frac{C_b}{\sqrt{k}}\hat{u}^2, \qquad (1)\\ \frac{\partial \hat{T}}{\partial \hat{t}} + v_0 \frac{\partial \hat{T}}{\partial \hat{y}} &= \frac{\kappa}{\rho C_p}\frac{\partial^2 \hat{T}}{\partial \hat{y}^2} + \frac{\mu}{\rho C_p}\left(1+\frac{1}{\beta}\right)\left(\frac{\partial \hat{u}}{\partial \hat{y}}\right)^2 - \frac{1}{\rho C_p}\frac{\partial q_r}{\partial \hat{y}} + \frac{\sigma B_0^2}{\rho C_p}\hat{u}^2\\ &\quad + \frac{Q_0}{\rho C_p}(\hat{T}-T_0) + \frac{Dk_T}{C_s C_p}\frac{\partial^2 \hat{C}}{\partial \hat{y}^2}, \qquad (2)\\ \frac{\partial \hat{C}}{\partial \hat{t}} + v_0 \frac{\partial \hat{C}}{\partial \hat{y}} &= D\frac{\partial^2 \hat{C}}{\partial \hat{y}^2} + \frac{Dk_T}{T_m}\frac{\partial^2 \hat{T}}{\partial \hat{y}^2} - k_1 \hat{C}, \qquad (3)\end{aligned}$$

where κ is the thermal conductivity, μ is the dynamic viscosity, σ is the electrical conductivity, ω is the frequency, ν is the kinematic viscosity, ρ is the density of the fluid, $\hat{T}$, $\hat{C}$ are the temperature and concentration of the fluid, $\hat{p}$ is pressure, $\varPhi$ and k are the porosity and permeability of porous medium, $\beta_{\hat{C}}$ is the coefficient of concentration expansion, D is the coefficient of mass diffusivity, k_1 is the 1st-order chemical reaction rate, $\hat{t}$ is time, $\beta_{\hat{T}}$ is the coefficient of thermal expansion, g is the acceleration due to gravity, $\beta = \mu_B\sqrt{2\pi_c}/P_{\hat{y}}$ is the Casson fluid parameter, T_m is the mean temperature of the fluid, k_T is the thermal diffusion ratio, C_s is the concentration susceptibility, q_r is the radiative heat flux, Q_0 is the coefficient of heat source/sink, C_b is the form of drag coefficient, C_p is the specific heat at constant pressure. Thermal radiation is simulated utilizing the Rosseland approximation (Makinde et al. [22]), and as per this, q_r is specified by

$$q_r = -\left(\frac{4\hat{\sigma}}{3\chi}\right)\frac{\partial \hat{T}^4}{\partial \hat{y}},$$

where χ and $\hat{\sigma}$ are the Rosseland mean absorption coefficient and Stefan–Boltzmann constant. Assuming an adequately small temperature difference in the flow and expanding $\hat{T}^4$ by Taylor's series about T_0, we get $\hat{T}^4 \cong 4T_0^3\hat{T} - 3T_0^4$ (higher-order terms are neglected). In view of q_r and $\hat{T}^4$, Eq. (2) becomes

$$\begin{aligned}\frac{\partial \hat{T}}{\partial \hat{t}} + v_0 \frac{\partial \hat{T}}{\partial \hat{y}} =& \frac{\kappa}{\rho C_p}\frac{\partial^2 \hat{T}}{\partial \hat{y}^2} + \frac{\mu}{\rho C_p}\left(1+\frac{1}{\beta}\right)\left(\frac{\partial \hat{u}}{\partial \hat{y}}\right)^2 + \frac{1}{\rho C_p}\frac{16\hat{\sigma}T_0^3}{3\chi}\frac{\partial^2 \hat{T}}{\partial \hat{y}^2}\\ &+ \frac{\sigma B_0^2}{\rho C_p}\hat{u}^2 + \frac{Q_0}{\rho C_p}(\hat{T}-T_0) + \frac{Dk_T}{C_s C_p}\frac{\partial^2 \hat{C}}{\partial \hat{y}^2}. \qquad (4)\end{aligned}$$

The boundary conditions are (Malathy et al. [23], Xinhui et al. [35])

$$\hat{u} = \frac{\sqrt{k}}{\alpha}\left(1+\frac{1}{\beta}\right)\left(\frac{\partial \hat{u}}{\partial \hat{y}}\right), \quad -\kappa\frac{\partial \hat{T}}{\partial \hat{y}} = h_f(\hat{T}-T_0), \quad \hat{C} = C_0 \quad \text{at } \hat{y} = 0,$$
$$\hat{u} = -\frac{\sqrt{k}}{\alpha}\left(1+\frac{1}{\beta}\right)\left(\frac{\partial \hat{u}}{\partial \hat{y}}\right), \quad -\kappa\frac{\partial \hat{T}}{\partial \hat{y}} = h_f(\hat{T}-T_1), \quad \hat{C} = C_1 \quad \text{at } \hat{y} = h,$$

where α and h_f are slip coefficient at the surface of the porous walls and heat coefficient, respectively.

The following dimensionless quantities are invoked:

$$x = \frac{\hat{x}}{h}, \qquad y = \frac{\hat{y}}{h}, \qquad u = \frac{\hat{u}}{U}, \qquad p = \frac{h\hat{p}}{\mu U},$$
$$\theta = \frac{\hat{T}-T_0}{T_1-T_0}, \qquad \phi = \frac{\hat{C}-C_0}{C_1-C_0}, \qquad t = \omega\hat{t}. \tag{5}$$

Using Eq. (5), Eqs. (1), (4), and (3) transformed to

$$H^2\frac{\partial u}{\partial t} + R\frac{\partial u}{\partial y} = -\frac{\partial p}{\partial x} + \left(1+\frac{1}{\beta}\right)\left(\frac{\partial^2 u}{\partial y^2}\right) + \frac{Gr}{Re}\theta + \frac{Gc}{Re}\phi$$
$$- \left(M^2 + \frac{1}{Da}\right)u - FsRe\,u^2, \tag{6}$$

$$H^2\frac{\partial \theta}{\partial t} + R\frac{\partial \theta}{\partial y} = \frac{1}{Pr}\left(1+\frac{4}{3}Rd\right)\frac{\partial^2\theta}{\partial y^2} + \left(1+\frac{1}{\beta}\right)Ec\left(\frac{\partial u}{\partial y}\right)^2$$
$$+ M^2Ec\,u^2 + Q\theta + Du\frac{\partial^2\phi}{\partial y^2}, \tag{7}$$

$$H^2\frac{\partial \phi}{\partial t} + R\frac{\partial \phi}{\partial y} = \frac{1}{Sc}\frac{\partial^2\phi}{\partial y^2} + Sr\frac{\partial^2\theta}{\partial y^2} - \gamma\phi - K_1, \tag{8}$$

where U is the characteristic velocity, θ, ϕ are dimensionless temperature and concentration, $H = h\sqrt{\omega}/\sqrt{\nu}$ is frequency parameter, $Gr = g\beta_{\hat{T}}(T_1-T_0)h^3/\nu^2$ is Grashof number, $Gc = g\beta_{\hat{C}}(C_1-C_0)h^3/\nu^2$ is solutal Grashof number, $Rd = 4\hat{\sigma}T_0^3/(\kappa\chi)$ is the radiation parameter, $Re = Uh/\nu$ is Reynolds number, $Pr = \mu C_p/\kappa$ is the Prandtl number, $M = B_0h\sqrt{\sigma}/\sqrt{\mu}$ is the Hartmann number, $Fs = C_bh/\sqrt{k}$ is the Forchheimer number, $Da = k/(\Phi h^2)$ is the Darcy number of the porous media, $Ec = U^2/[C_p(T_1-T_0)]$ is the Eckert number, $Q = Q_0h^2/[(\rho C_p)\nu]$ is heat source/sink parameter, $R = v_0h/\nu$ is cross flow Reynolds number, $Sr = Dk_T(T_1-T_0)/[T_m\nu(C_1-C_0)]$ is the Soret number, $\gamma = k_1h^2/\nu$ is the chemical reaction parameter, $Sc = \nu/D$ is the Schmidt number, $Du = Dk_T(C_1-C_0)/[C_sC_p\nu(T_1-T_0)]$ is the Dufour number, and $K_1 = k_1C_0h^2/[\nu(C_1-C_0)]$.

The corresponding boundary conditions are

$$u = L\left(1+\frac{1}{\beta}\right)\left(\frac{\partial u}{\partial y}\right), \quad \frac{\partial \theta}{\partial y} = -B_i\theta, \quad \phi = 0 \quad \text{at } y = 0,$$
$$u = -L\left(1+\frac{1}{\beta}\right)\left(\frac{\partial u}{\partial y}\right), \quad \frac{\partial \theta}{\partial y} = -B_i(\theta - 1), \quad \phi = 1 \quad \text{at } y = 1,$$

where $B_i = h_f h/\kappa$ is the heat transfer Biot number, and $L = \sqrt{k}/(\alpha h)$ is the slip parameter.

3 Solution of the problem

To acquire the solution of Eqs. (6)–(8), a perturbative solution has been assumed in the following form:

$$\begin{aligned} -\frac{\partial p}{\partial x} &= A_0 + \varepsilon A_1 \mathrm{e}^{\mathrm{i}t}, & \theta(y,t) &= \theta_0(y) + \varepsilon\theta_1(y)\mathrm{e}^{\mathrm{i}t}, \\ u(y,t) &= u_0(y) + \varepsilon u_1(y)\mathrm{e}^{\mathrm{i}t}, & \phi(y,t) &= \phi_0(y) + \varepsilon\phi_1(y)\mathrm{e}^{\mathrm{i}t} \end{aligned} \tag{9}$$

and neglecting higher orders. Here ϵ is the suitably chosen positive quantity, $\phi_1(y)$ is unsteady concentration profile, $\theta_1(y)$ is unsteady temperature profile, $u_1(y)$ is unsteady velocity profile, $\phi_0(y)$ is steady concentration profile, $\theta_0(y)$ is steady temperature profile, $u_0(y)$ is steady velocity profile, u is nondimensional velocity, and A_0, A_1 are positive constants.

Substituting Eq. (9) into Eqs. (6)–(8) and comparing the coefficients of various powers of ε, we obtain

$$\begin{aligned} &\left(1+\frac{1}{\beta}\right)u_0'' - Ru_0' - \left(M^2 + \frac{1}{Da}\right)u_0 \\ &\quad = -A_0 - \frac{Gr}{Re}\theta_0 - \frac{Gc}{Re}\phi_0 + FsRe\,u_0^2, \end{aligned} \tag{10}$$

$$\begin{aligned} &\left(1+\frac{1}{\beta}\right)u_1'' - Ru_1' - \left(M^2 + \frac{1}{Da} + \mathrm{i}H^2\right)u_1 \\ &\quad = -A_1 - \frac{Gr}{Re}\theta_1 - \frac{Gc}{Re}\phi_1 + 2FsRe\,u_0u_1, \end{aligned} \tag{11}$$

$$\begin{aligned} &\left(1+\frac{4}{3}Rd\right)\theta_0'' - RPr\,\theta_0' + QPr\,\theta_0 \\ &\quad = -\left(1+\frac{1}{\beta}\right)Ec\,Pr\,u_0'^2 - M^2 Ec\,Pr\,u_0^2 - DuPr\,\phi_0'', \end{aligned} \tag{12}$$

$$\begin{aligned} &\left(1+\frac{4}{3}Rd\right)\theta_1'' - RPr\,\theta_1' + \left(QPr - \mathrm{i}H^2 Pr\right)\theta_1 \\ &\quad = -2\left(1+\frac{1}{\beta}\right)Ec\,Pr\,u_0'u_1' - 2M^2 Ec\,Pr\,u_0u_1 - DuPr\,\phi_1'', \end{aligned} \tag{13}$$

$$\phi_0'' - RSc\,\phi_0' - \gamma Sc\,\phi_0 = -Sc\,Sr\,\theta_0'' + K_1 Sc, \tag{14}$$
$$\phi_1'' - RSc\,\phi_1' - \left(\mathrm{i}H^2 Sc + \gamma Sc\right)\phi_1 = -Sc\,Sr\,\theta_1''. \tag{15}$$

The corresponding boundary conditions are

$$\begin{aligned}
&u_0(0) = L\left(1+\frac{1}{\beta}\right)u_0'(0), && u_0(1) = -L\left(1+\frac{1}{\beta}\right)u_0'(1),\\
&u_1(0) = L\left(1+\frac{1}{\beta}\right)u_1'(0), && u_1(1) = -L\left(1+\frac{1}{\beta}\right)u_1'(1);\\
&\theta_0'(0) = -B_i\left[\theta_0(0)-1\right], && \theta_0'(1) = -B_i\theta_0(1),\\
&\theta_1'(0) = -B_i\theta_1(0), && \theta_1'(1) = -B_i\theta_1(1);\\
&\phi_0(0) = 0, \quad \phi_0(1) = 1, && \phi_1(0) = 0, \quad \phi_1(1) = 0.
\end{aligned} \tag{16}$$

Further, the dimensionless Nusselt and Sherwood numbers at the walls are given by

$$Nu = -\frac{\partial\theta}{\partial y}\bigg|_{y=0,1} \quad \text{and} \quad Sh = -\frac{\partial\phi}{\partial y}\bigg|_{y=0,1}.$$

It is noted that the system of ODEs (10)–(15) along with associated boundary conditions (16) is nonlinear and coupled. We have employed the 4th-order Runge–Kutta technique together with shooting method for finding the numerical solution. Throughout the calculations, the employed parametric values $Du = 0.03$, $A_0 = 1$, $Sr = 2$, $\beta = 2$, $B_i = 1$, $A_1 = 1$, $\gamma = 1$, $Gr = 7$, $Rd = 2$, $Q = -1$, $Da = 0.5$, $L = 0.06$, $R = 1$, $t = \pi/4$, $H = 2$, $Sc = 0.65$, $\varepsilon = 0.01$, $Gc = 7$, $Re = 3$, $Pr = 21$, $Ec = 0.5$, $K_1 = 0.001$, $M = 2$, $Fs = 0.5$, unless otherwise stated.

4 Results and discussion

The influences of various physical parameters on velocity, temperature, concentration profiles are elucidated graphically in Figs. 2–5. Figures 2(a)–2(f) describe the impact of the slip parameter (L), Darcy number of the porous media (Da), Casson fluid parameter (β), Hartmann number (M), Forchheimer number (Fs), and Grashof number (Gr) on the velocity profile. Figure 2(a) reveals that an increase in L results in rise of velocity profile. Figure 2(b) elucidates that the velocity increases with an enhancing Darcy number. Figures 2(c) and 2(f) depict that there is an enhancement in velocity with an enhancing Casson fluid parameter and Grashof number. Figure 2(d) depicts that for a rise in M, there is a decrease in velocity. This can be because of Lorentz forces created by the applied magnetic field act as resistive drag forces opposite to the flow direction. Hence there is a decrease in velocity. Figure 2(e) delineates that a rise in Forchheimer number creates a resistance in fluid flow which results an abatement in velocity.

The variation of temperature distribution (θ) for various values of B_i, Rd, Du, and Sr are shown in Figs. 3(a)–3(d). Figure 3(a) illustrates the influence of B_i on θ. It is observed that for a given rise Biot number, there is a decrease in the temperature. A superior value

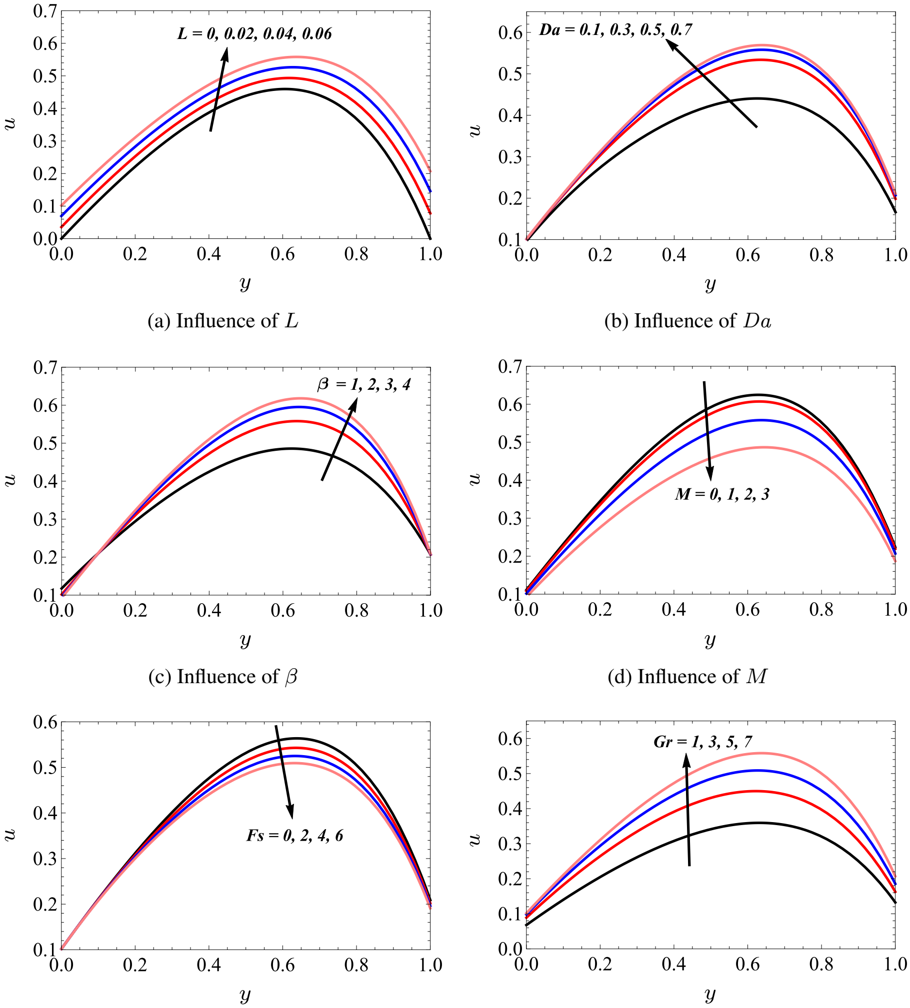

(a) Influence of L (b) Influence of Da

(c) Influence of β (d) Influence of M

(e) Influence of Fs (f) Influence of Gr

Figure 2. Velocity distributions.

of B_i includes a higher degree of convective cooling at the channel walls, subsequently inflicting lower temperature at the channel walls and additionally within the bulk fluid. It is predictable that as $B_i \to \infty$, the convective boundary conditions will turn into the prescribed wall temperatures. Figure 3(b) depicts the effect of thermal radiation parameter on θ. It is observed that θ increases with an enhancement of Rd. This phenomenon can be ascribed to the physical fact that the thermal boundary layer thickness rises with an enhancing Rd. The variation of temperature with respect to the Dufour number is shown in Fig. 3(c). It is seen that there is an enhancement in temperature with an enhancing of Du. Actually, Du is associated in energy flux caused by a concentration gradient.

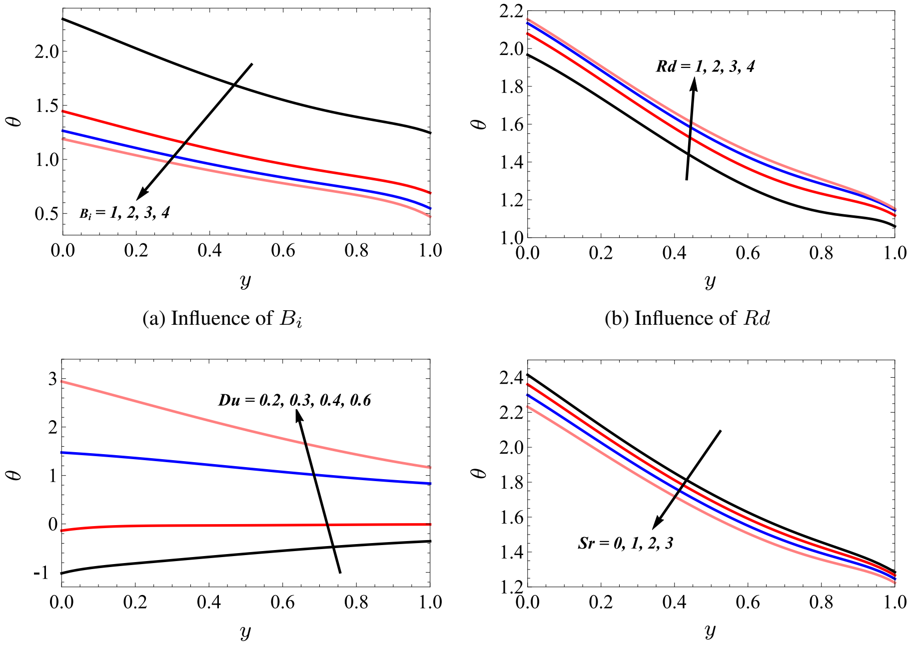

(a) Influence of B_i (b) Influence of Rd

(c) Influence of Du (d) Influence of Sr

Figure 3. Temperature distributions.

Subsequently, bigger concentration gradient cause to rise the temperature. Figure 3(d) reveals that an increase in Sr results in decrease of temperature distribution.

Figure 4 illustrates the influences of Sc, Sr, and γ on concentration distribution. Figure 4(a) exhibits that the concentration profile decreases for given rise in Schmidt number. This is observed due to a rise in Sc that it turn makes the concentration boundary layer thinner than momentum boundary layer. Figure 4(b) depicts the influence of Soret number on ϕ. One can infer that ϕ is enhanced with increasing Sr. Figure 4(c) depicts γ effect on concentration. It is seen that the concentration falls with a rise in the destructive chemical reaction ($\gamma > 0$). The contrary pattern can be noticed for the case of generative chemical reaction ($\gamma < 0$). The effect of Du and Sr on the temperature and concentration distributions is shown in Figs. 5(a)–5(b). Figure 5(a) elucidates that a rise in Du with a decrease in Sr rises the thermal boundary layer growth. It is noticed from Fig. 5(b) that a decrease in Sr with a rise in Du has the tendency to decrease the concentration distribution. Physically, Soret effect reports that mass flux is made once a system is underneath a temperature gradient. Further, a rise in Du improves the convention velocity over combined influences of thermal and solutal buoyancy forces that leads to enhance the heat transfer but fall the mass transfer of the fluid.

The present numerical values corresponding to the Nusselt number compared with the previously published numerical results of Kumar et al. [19] are shown in Table 1. This comparison shows that the present results in limiting case are in good agrement with the

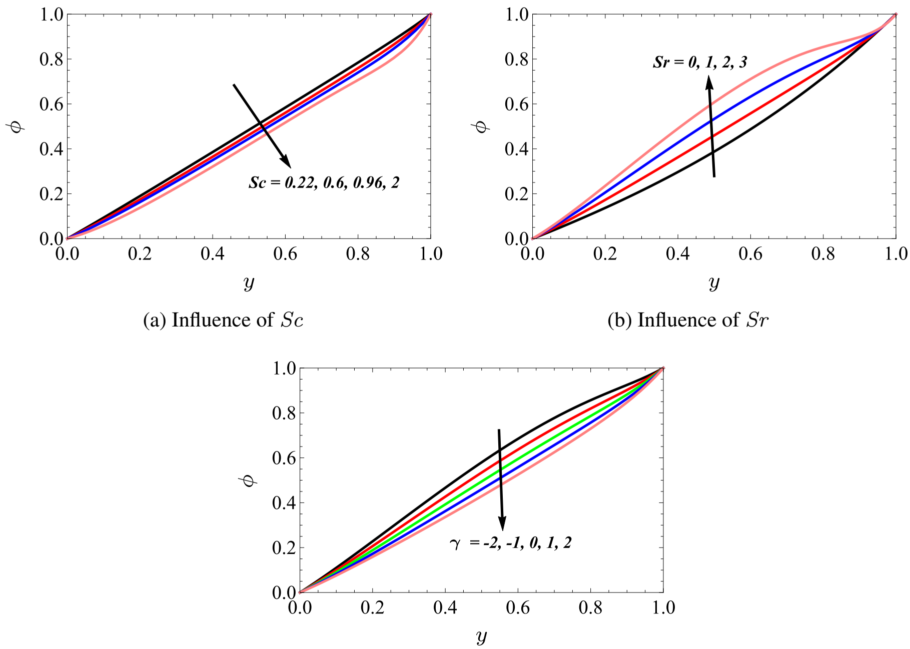

(a) Influence of Sc

(b) Influence of Sr

(c) Influence of γ.

Figure 4. Concentration distributions.

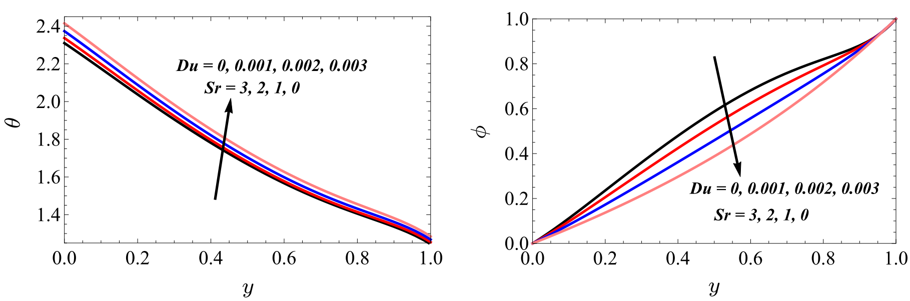

(a) Temperature

(b) Concentration

Figure 5. Effect of Du and Sr on the temperature and concentration distributions.

published results. Table 2 compares the findings obtained by an analytical method (double perturbation) with the results obtained by a numerical method (4th-order R–K method together with shooting technique) to verify the validity of the current model. Table 3 shows the variations in Nu and Sh for different values of Fs, β, B_i, Du, Sr, and Sc. The Nusselt and Sherwood numbers at the left and right walls are denoted by Nu_0, Nu_1, and Sh_0, Sh_1, respectively. It is noticed that Nu falls with a rise in Forchheimer number at the left wall, while it rises at the right wall. The Nusselt number rises at both walls by

Table 1. Comparison of results of Nusselt number for several values of Casson fluid parameter in the absence of Brownian motion parameter, thermophoresis parameter, Lewis number, Dufour number, cross flow Reynolds number, Forchheimer number, slip parameter, and the heat transfer Biot number.

β	Kumar et al. [19]		Present	
	Nu_0	Nu_1	Nu_0	Nu_1
2	6.00734	−5.80169	6.00734	−5.80169
3	5.37199	−5.13925	5.37199	−5.13925

Table 2. Comparison of the analytical results with the numerical results by taking $R = Fs = Du = B_i = Ec = 0$.

S. No.	y	Analytical method			Numerical method		
		$u(y)$	$\theta(y)$	$\phi(y)$	$u(y)$	$\theta(y)$	$\phi(y)$
1	0.1	0.2096	0.0648	0.1112	0.2095	0.0648	0.1112
2	0.3	0.4045	0.2019	0.3317	0.4045	0.2019	0.3317
3	0.5	0.5366	0.3624	0.5456	0.5367	0.3624	0.5456
4	0.7	0.5562	0.5647	0.7465	0.5561	0.5647	0.7465
5	0.9	0.3901	0.8324	0.9243	0.3901	0.8324	0.9243

Table 3. Effect of Fs, β, B_i, Du, Sr, Sc on Nusselt and Sherwood number distributions when $A_0 = 1$, $A_1 = 1$, $\gamma = 1$, $Gr = 7$, $Rd = 2$, $Q = -1$, $Da = 0.5$, $L = 0.06$, $R = 1$, $t = \pi/4$, $H = 2$, $\varepsilon = 0.01$, $Gc = 7$, $Re = 3$, $Pr = 21$, $Ec = 0.5$, $K_1 = 0.001$, $M = 2$.

Parameter	Values	Nu_0	Nu_1	Sh_0	Sh_1
Fs	0	0.75329	−0.83727	0.43837	3.42651
	2	0.69289	−0.82247	0.41899	3.30946
	4	0.64031	−0.81183	0.40492	3.21333
	6	0.59371	−0.80410	0.39459	3.13252
β	1	0.65735	−0.75266	0.33749	3.08491
	2	0.73733	−0.83309	0.43291	3.39487
	3	0.77105	−0.88217	0.49110	3.56435
	4	0.79022	−0.91441	0.52927	3.67176
B_i	1	−1.29919	−1.24512	0.87477	1.78748
	2	−0.89213	−1.37839	0.78766	2.36379
	3	−0.79586	−1.63896	0.73488	2.75861
	4	−0.75594	−1.87780	0.69815	3.07305
Du	0.2	2.01968	0.35629	−1.05216	1.98978
	0.3	1.13861	0.00978	−0.61865	1.74097
	0.4	−0.47402	−0.45283	0.14213	0.63832
	0.6	−1.94072	−1.16345	0.77237	0.74398
Sr	0	−1.41501	−1.28365	0.63868	1.56538
	1	−1.36021	−1.26557	0.77031	1.66325
	2	−1.29919	−1.24512	0.87477	1.78748
	3	−1.23228	−1.22238	0.94845	1.94132
Sc	0.22	−1.36315	−1.26158	0.91487	1.22006
	0.60	−1.36069	−1.26512	0.78584	1.61082
	0.96	−1.35638	−1.26838	0.68012	1.99382
	2.00	−1.33341	−1.27630	0.42877	3.17415

rising Sr, whereas it falls at both walls by rising Du. One can observe that at the left wall, Nu enhances with a rise in the β, B_i, and Sc, while it falls at the right wall. One can infer that at both walls, Sh rises by rising β and Sr, while it falls at both walls by increasing Fs. It can be noticed that Sh decreases with an increase in B_i and Sc at the left wall, whereas it rises at the right wall. The reverse trend can be seen for the case of Dufour number.

5 Conclusions

An analysis is made on pulsating MHD slip flow of Casson fluid in a vertical non-Darcian porous space with convective boundary condition. The considered investigation is significant as flow of Casson fluids (drilling muds, greases, clay coating, certain oils, numerous impulsions, and blood) in porous channel are utilized in modelling biological and science research. The analytical and numerical solutions are constructed for flow variables. The salient points of this investigation are as follows:

- The velocity increases with an increasing slip and Casson fluid parameter, while it falls with an enhancing Forchheimer number.
- It is noticed that the temperature rises with an enhancing Dufour number and radiation parameter, while it falls with an enhancing Soret number.
- Temperature enhances for a given rise in Dufour number with a decrease in Soret number.
- Concentration falls by enhancing Schmidt number and rises by rising the Soret number.
- Nusselt number escalates with the increase in Casson fluid parameter and heat transfer Biot number at the left wall, while it is a decreasing function at right wall.
- Sherwood number rises at the both walls for a given increase in Casson fluid parameter and Soret number.

References

1. S.O. Adesanya, J.A. Falade, O.D. Makinde, Pulsating flow through vertical porous channel with viscous dissipation effect, *U.P.B. Sci. Bull., Ser. D*, **77**(1):25–36, 2015, https://www.scientificbulletin.upb.ro/rev_docs_arhiva/fulldb6_966044.
2. S.O. Ajadi, A note on the unsteady flow of dusty viscous fluid between two parallel plates, *J. Appl. Math. Comput.*, **18**:393–403, 2005, https://doi.org/10.1007/BF02936582.
3. R. Bhargava, H.S. Takhar, S. Rawat, T.A. Beg, O.A. Beg, Finite element solutions for non-Newtonian pulsatile flow in a non-darcian porous medium conduit, *Nonlinear Anal. Model. Control*, **12**(3):317–327, 2007, https://doi.org/10.15388/NA.2007.12.3.14690.
4. N. Casson, A flow equation for the pigment oil suspensions of the printing ink type, in C.C. Mill (Ed.), *Rheology of Disperse Systems*, Pergamon, New York, 1959, pp. 84–102.

5. M. Celli, A.V. Kuznetsov, A new mechanism for buoyancy driven convection in pulsating viscous flows: A theoretical study, *Int. J. Heat Mass Transfer*, **118**:340–348, 2018, https://doi.org/10.1016/j.ijheatmasstransfer.2017.10.112.
6. A.J. Chamkha, Flow of two-immiscible fluids in porous and nonporous channels, *J. Fluids Eng.*, **122**(1):117–124, 2000, https://doi.org/10.1115/1.483233.
7. A.J. Chamkha, On laminar hydromagnetic mixed convection flow in a vertical channel with symmetric and asymmetric wall heating conditions, *Int. J. Heat Mass Transfer*, **45**:2509–2525, 2002, https://doi.org/10.1016/S0017-9310(01)00342-8.
8. A.J. Chamkha, T. Grosan, I. Pop, Fully developed free convection of a micropolar fluid in a vertical channel, *Int. Commun. Heat Mass Transfer*, **29**(8):1119–1127, 2002, https://doi.org/10.1016/S0735-1933(02)00440-2.
9. T. Chinyoka, O.D. Makinde, Analysis of transient generalized couette flow of a reactive variable viscosity third-grade liquid with asymmetric convective cooling, *Math. Comput. Modelling*, **54**(1–2):160–174, 2011, https://doi.org/10.1016/j.mcm.2011.01.047.
10. R.K. Dash, K.N. Mehta, G. Jayaraman, Casson fluid flow in a pipe filled with a homogeneous porous medium, *Int. J. Eng. Sci.*, **34**(10):1145–1156, 1996, https://doi.org/10.1016/0020-7225(96)00012-2.
11. N.F. Dzulkifli, N. Bachok, I. Pop, N.A. Yacob, N.Md. Arifin, H. Rosali, Soret and Dufour effects on unsteady boundary layer flow and heat transfer of nanofluid over a stretching/shrinking sheet: A stability analysis, *J. Chem. Eng. Process Technol.*, **8**(3):1–9, 2017, https://doi.org/10.4172/2157-7048.1000336.
12. K. Haddad, O. Ertunc, M. Mishra, A. Delgado, Pulsating laminar fully developed channel and pipe flows, *Phys. Rev. E*, **81**(1):016303, 2010, https://doi.org/10.1103/PhysRevE.81.016303.
13. A.S. Idowu, B.O. Falodun, Soret–Dufour effects on MHD heat and mass transfer of Walter's-B viscoelastic fluid over a semi-infinite vertical plate: spectral relaxation analysis, *J. Taibah Univ. Sci.*, **13**(1):49–62, 2018, https://doi.org/10.1080/16583655.2018.1523527.
14. A. Khalid, I. Khan, A. Khan, S. Shafie, Unsteady MHD free convection flow of Casson fluid past over an oscillating vertical plate embedded in a porous medium, *Eng. Sci. Technol. Int. J.*, **18**:309–317, 2015, https://doi.org/10.1016/j.jestch.2014.12.006.
15. M.I. Khan, T. Hayat, S. Afzal, M.I. Khan, A. Alsaedi, Theoretical and numerical investigation of Carreau-Yasuda fluid flow subject to Soret and Dufour effects, *Comput. Methods Programs Biomed.*, **186**:105145, 2020, https://doi.org/10.1016/j.cmpb.2019.105145.
16. C.K. Kumar, S. Srinivas, Simultaneous effects of thermal radiation and chemical reaction on hydromagnetic pulsatile flow of a Casson fluid in a porous space, *Eng. Trans.*, **65**(3):461–481, 2017, https://et.ippt.gov.pl/index.php/et/article/view/400.
17. C.K. Kumar, S. Srinivas, Influence of joule heating and thermal radiation on unsteady hydromagnetic flow of chemically reacting Casson fluid over an inclined porous stretching sheet, *Spec. Top. Rev. Porous Media*, **10**(4):385–400, 2019, https://doi.org/10.1615/SpecialTopicsRevPorousMedia.2019026908.
18. C.K. Kumar, S. Srinivas, Pulsating hydromagnetic flow of Casson fluid in a vertical channel filled with non-Darcian porous medium, *Heat Transfer*, **50**(6):5225–5239, 2021, https://doi.org/10.1002/htj.22121.

19. C.K. Kumar, S. Srinivas, A.S. Reddy, MHD pulsating flow of Casson nanofluid in a vertical porous space with thermal radiation and joule heating, *J. Mech.*, **36**(4):535–549, 2020, https://doi.org/10.1017/jmech.2020.5.
20. J.P. Kumar, J.C. Umavathi, A.J. Chamkha, I. Pop, Fully-developed free-convective flow of micropolar and viscous fluids in a vertical channel, *Appl. Math. Modelling*, **34**(5):1175–1186, 2010, https://doi.org/10.1016/j.apm.2009.08.007.
21. P. Loganathan, K. Deepa, Computational exploration of Casson fluid flow over a Riga-plate with variable chemical reaction and linear stratification, *Nonlinear Anal. Model. Control,*, **25**(3):443–460, 2020, https://doi.org/10.15388/namc.2020.25.16659.
22. O.D. Makinde, M.G. Reddy, K.V. Reddy, Effects of thermal radiation on MHD peristaltic motion of Walters-B fluid with heat source and slip conditions, *J. Appl. Fluid Mech.*, **10**(4):1105–1112, 2017, https://doi.org/10.18869/ACADPUB.JAFM.73.241.27082.
23. T. Malathy, S. Srinivas, A.S. Reddy, Chemical reaction and thermal radiation effects on MHD pulsatile flow of an Oldroyd-B fluid in a porous medium with slip and convective boundary conditions, *J. Porous Media*, **20**(4):287–301, 2017, https://doi.org/10.1615/JPorMedia.v20.i4.10.
24. D. Pal, G. Mandal, K. Vajravelu, Soret and Dufour effects on MHD convective-radiative heat and mass transfer of nanofluids over a vertical non-linear stretching/shrinking sheet, *Appl. Math. Comput.*, **287-288**:184–200, 2016, https://doi.org/10.1016/j.amc.2016.04.037.
25. A. Pantokratoras, Natural convection over a vertical isothermal plate in a non-Newtonian power-law fluid: New results, *Adv. Mech. Eng.*, **8**(5):1–12, 2016, https://doi.org/10.1177/1687814016644111.
26. G. Radhakrishnamacharya, M.K. Maiti, Heat transfer to pulsatile flow in a porous channel, *Int. J. Heat Mass Transfer*, **20**(2):171–173, 1977, https://doi.org/10.1016/0017-9310(77)90009-6.
27. M. Sajid, M. Awais, S. Nadeem, T. Hayat, The influence of slip condition on thin film flow of a fourth grade fluid by the homotopy analysis method, *Comput. Math. Appl.*, **56**:2019–2026, 2008, https://doi.org/10.1016/j.camwa.2008.04.022.
28. H.M. Sayed, E.H. Aly, K. Vajravelu, Influence of slip and convective boundary conditions on peristaltic transport of non-Newtonian nanofluids in an inclined asymmetric channel, *Alexandria Eng. J.*, **55**:2209–2220, 2016, https://doi.org/10.1016/j.aej.2016.04.041.
29. S. Shateyi, S.S. Motsa, P. Sibanda, The effects of thermal radiation, hall currents, Soret, and Dufour on MHD flow by mixed convection over a vertical surface in porous media, *Math. Probl. Eng.*, **2010**:Article ID 627475, 2010, https://doi.org/10.1155/2010/627475.
30. S. Srinivas, C.K. Kumar, A.S. Reddy, Pulsating flow of Casson fluid in a porous channel with thermal radiation, chemical reaction and applied magnetic field, *Nonlinear Anal. Model. Control*, **23**(2):213–233, 2018, https://doi.org/10.15388/NA.2018.2.5.
31. S. Srinivas, T. Malathy, A.S. Reddy, A note on thermal-diffusion and chemical reaction effects on MHD pulsating flow in a porous channel with slip and convective boundary conditions, *J. King Saud Univ., Eng. Sci.*, **28**(2):213–221, 2016, https://doi.org/10.1016/j.jksues.2014.03.011.

32. J.C. Umavathi, A.J. Chamkha, Stability analysis of cross diffusion for the walters B fluid model saturated with permeable nanofluid, *J. Therm. Sci. Eng. Appl.*, **11**(4):041014, 2019, https://doi.org/10.1115/1.4044078.

33. W.P. Walawender, T.Y. Chen, D.F. Cala, An approximate Casson fluid model for tube flow of blood, *Biorheology*, **12**(2):111–119, 1975, https://doi.org/10.3233/bir-1975-12202.

34. C.Y. Wang, Pulsatile flow in a porous channel, *J. Appl. Mech.*, **38**(2):553–555, 1971, https://doi.org/10.1115/1.3408822.

35. S. Xinhui, Z. Liancun, C. Xuehui, Z. Xinxin, C. Limer, L. Min, The effects of slip velocity on a micropolar fluid through a porous channel with expanding or contracting walls, *Comput. Methods Biomech. Biomed. Eng.*, **17**(4):423–432, 2014, https://doi.org/10.1080/10255842.2012.688108.